Building and Environment 129 (2018) 142–153

Contents lists available at ScienceDirect

Building and Environment

journal homepage: www.elsevier.com/locate/buildenv

Vertical ventilation concepts for future passenger cars

Tobias Dehne*, Pascal Lange, André Volkmann, Daniel Schmeling, Mikhail Konstantinov, Johannes Bosbach

Institute of Aerodynamics and Flow Technology, German Aerospace Center, Göttingen, Germany

ARTICLE INFO

Keywords:
Passenger car ventilation
Thermal passenger comfort
Vertical ventilation
Temperature control efficiency
Equivalent temperature
Computational fluid dynamics

ABSTRACT

We compared three vertical ventilation concepts to dashboard ventilation in a generic car cabin with the aim to improve thermal passenger comfort and energy efficiency of future cars. Temperatures were analyzed with an infrared camera and local temperature sensors. Omnidirectional velocity probes were used to capture the fluid velocities and temperatures in the vicinity of thermal passenger dummies, which were used to simulate the thermal impact of the passengers. Further, the ventilation efficiency was measured with the tracer gas technique using humidity sensors in the vicinity of the dummies and in the air outlets. Besides the experimental investigations, the relevant flow cases were studied by Computational Fluid Dynamics simulations using the RANS method, providing insight into the complex and three-dimensional flow structures of the passenger compartment. Validation of the simulations with the experimental data revealed acceptable consistency, however, with local deviations indicating further need for experimental investigations. The ventilation efficiencies of the vertical ventilation concepts were at least comparable or even better as compared to dashboard ventilation. Regarding the comfort-relevant flow parameters, dashboard ventilation stood out with the lowest temperature stratification but revealed comfort-critical flow velocities. The vertical ventilation concepts allowed for comfortable velocities, but tended to produce comfort-critical temperature stratifications. Pursuing the equivalent temperatures, the vertical systems revealed an improved heating performance over dashboard ventilation. During summer and spring/fall conditions, low momentum ceiling ventilation as well as the combination of cabin displacement ventilation and low momentum ceiling ventilation were able to provide comfortable equivalent temperature distributions.

1. Introduction

Nowadays, car manufacturers are faced with several challenges regarding successful commercialization of modern electric vehicles (EVs) [1]. Particularly, the restricted cruising range is one of the biggest concerns influencing the consumer decision to purchase EVs [2]. To overcome this limitation for the majority of user profiles, not only the development of the latest battery technology, but also the optimization of the energy consumption of the different sub-systems is mandatory. In this context, the air-conditioning system (i.e., cooling and heating) should be noted as a serious reason for battery depleting which may easily lead to a reduction of the cruising range by as much as 33% [3]. Depending on the actual route profile, under extreme outdoor conditions even more than 65% of the energy use may be consumed for passenger heating, as observed in laboratory and field tests [4]. Energy-efficient heating systems in turn promise a reduction of energy consumption of the HVAC system by 50% [5]. Hence, increasing the heating and cooling efficiency is one part of our motivation to investigate vertical ventilation concepts. Further, with regard to autonomous driving, which is anticipated of future cars, allowing the front seats to be rotated backwards [6,7], vertical ventilation systems are appealing by allowing flexible cabin usage layouts in innovative vehicle concepts. Herewith, the requirements regarding ventilation efficiency and thermal passenger comfort of the novel systems have to be ensured. In addition to the aforementioned facts, with a significant amount of time spent traveling by car, the continuous improvement of passenger comfort has become an important criterion in terms of marketing of modern cars as well [8].

In the past, characterization and improvement of the performance of car ventilation with respect to thermal passenger comfort and energy efficiency was subject of several research studies, see e.g. Refs. [9–12]. In mixing ventilation, which is currently state of the art, the underlying fluid-dynamic processes are governed by the propagation of the incoming air jets inside the cabin, which can be accessed using optical field measurement techniques. Particle Image Velocimetry measurements of the flow velocity fields initiated by panel, defrost and foot-

* Corresponding author.
E-mail address: tobias.dehne@dlr.de (T. Dehne).

https://doi.org/10.1016/j.buildenv.2017.11.024
Received 24 August 2017; Received in revised form 26 October 2017; Accepted 16 November 2017
Available online 21 November 2017
0360-1323/ © 2017 Elsevier Ltd. All rights reserved.

ventilation inside of a real car cabin have been performed e.g. by Lee et al. [9]. However, the thermal passenger comfort is determined by the resulting enthalpy fluxes, which cannot be determined from velocity field measurements alone. Hereto, either combinations of local fluid temperature and velocity measurements or acquisition of integral quantities like equivalent temperatures are required [13]. Besides the static performance, the dynamic behavior is of high relevance as well. Hereto, Rosendahl et al. analyzed the heat-up process in a car cabin under winter conditions performing air-temperature, operating-temperature and equivalent-temperature measurements [10]. To determine thermal passenger comfort by means of local equivalent temperatures, measurement systems based on heated mannequins were employed as well [11]. Besides the thermal comfort, the air quality, which is considered as a result of the ventilation efficiency, is a parameter of utmost importance [8,14]. Herewith, not only the global performance, but also the local distribution of fresh air in the cabin is an issue. For example in a study of Wesseling et al., the ventilation efficiency in a real car cabin revealed significantly better values at the driver position in comparison with the passengers seated in the back [12]. Provided the requirements for air quality and thermal passenger comfort are ensured, novel or alternative variants of cabin ventilation have the prospect of improved heating and cooling efficiency: Studies in aircraft cabins reveal a potential to improve the heat removal efficiency by 75% using a hybrid combination of cabin displacement and ceiling-based displacement ventilation while even improving the thermal passenger comfort [15]. An issue of high relevance in aircraft cabins is, of course, the dispersal of carbon dioxide and pathogens involving numerical and experimental studies in cabin mock-ups [16,17]. Moreover, benefits were found with respect to CO_2 concentrations and relative humidity for alternative, i.e. personalized and displacement ventilation systems [18]. Previous studies of vertical ventilation concepts in a generic car cabin (GCC) demonstrate the potential of optimized thermal passenger comfort and an efficient use of energy [19–21]. Hereto, vertical ventilation concepts were analyzed experimentally with local temperature and velocity probes as well as numerically by means of coupled CFD and thermal comfort simulations and compared to a simplified dashboard ventilation. In these studies, cabin displacement ventilation (CDV) stood out with a high heat removal efficiency and a comfortable velocity distribution. However, comfort-critical temperature stratifications were observed, too. Only a combination of CDV with a low momentum ceiling ventilation was able to provide a presumably comfortable thermal environment under spring/fall conditions [20]. Hence, further investigations of vertical ventilation concepts are necessary, especially under consideration of integral comfort measures, such as the equivalent temperature [10,13]. A study related to ours addressed the ventilation of the rear cabin of a mini-bus cabin using low-momentum roof air outlets in combination with different air exhaust openings by means of CFD simulations [22]. However, no internal heat loads were considered, which are known to govern the flow in low momentum ventilation systems by means of thermal convection. Hence, the transferability of the results to the environment considered in our study is quite limited.

The thermal interaction of passenger cars with the surrounding is much more intense and complex as compared to aircraft cabins, involving a higher fraction of solar radiation and consideration of both, heating and cooling scenarios [23]. Hence, to make the advantages, which were found for alternative ventilation systems in aircraft cabins, accessible to passenger cars, further studies are required.

Hereto, this paper refers to a study conducted in the framework of the “next generation car (NGC)” project at the DLR. We investigated the cabin ventilation of a 1:1 full-scale GCC with a jacket heating/cooling system based on capillary tubes to investigate the steady performance under winter, spring/fall and summer conditions. Four thermal passenger dummies (TPDs) were used to simulate the impact of real passengers and as a measuring system to capture equivalent temperatures. During this stage of the project, the impact of solar radiation was not yet included.

Cabin displacement ventilation (CDV), low momentum ceiling ventilation (LMCV) and a hybrid case (HV), which combined CDV and LMCV, were experimentally compared to mixing ventilation (MV), represented by a generic dashboard ventilation, in the GCC. One focus was the local and global ventilation efficiencies measured under spring/fall conditions using water as tracer gas. In addition, the different ventilation concepts were compared regarding the thermal comfort with local temperature and velocity probes. Statements concerning the thermal passenger comfort using equivalent temperatures were derived experimentally and numerically from thermal passenger dummies under winter, spring/fall and summer conditions. Further, a detailed validation of CFD with experimental results, which had been lacking in previous studies [19–21], was conducted.

2. Materials and methods

2.1. Ventilation concepts in the generic car cabin

The generic car cabin provides three different ventilation systems, which can be used either individually or combined. Nowadays, mixing ventilation is the standard for ventilation of passenger compartments in cars. It is characterized by a high degree of mixing of the cabin air. Typically, jets of fresh air enter the cabin at well-defined positions, e.g. in the dashboard, and leave it in the luggage compartment. As a consequence of the large momentum of the incoming air, high flow

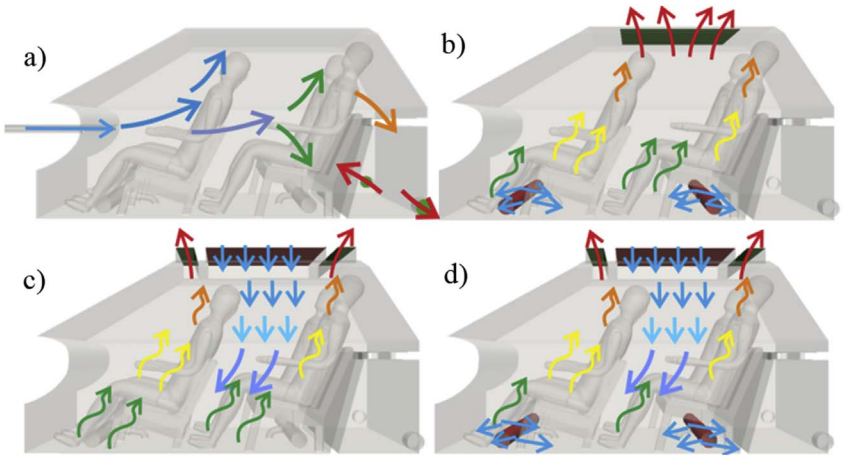

Fig. 1. Illustration of investigated ventilation systems in the GCC. a) mixing ventilation (MV), b) cabin displacement ventilation (CDV), c) low momentum ceiling ventilation (LMCV) and d) hybrid ventilation (HV) as a combination of CDV and LMCV.

velocities occur, which are prone to cause draft. A generic MV system was embodied in the GCC by four circular air supply tubes (length/diameter = 23) in the dashboard, oriented in longitudinal car direction (Fig. 1a). They generate undisturbed circular air jets oriented in longitudinal car direction, similar to a fully opened configuration of air inlet grilles in a commercial car. We preferred this configuration as opposed to a possibly more realistic setup with real air grilles, as, on the one hand, we wanted to work with well-defined boundary conditions that can be implemented in the CFD simulations unambiguously. On the other hand, we wanted to produce general results, independent of any OEM-specific influence. Hence, one should keep in mind that our MV baseline is just to be considered as one possible, even if not uncommon MV configuration and not an MV variant that is optimized in any way. Even if nowadays automatic switching between the most appropriate nozzle combinations as a function of the actual current weather conditions is technically possible for MV, this is still a quite uncommon feature, in the majority of consumer cars.

Three different vertical ventilation concepts are investigated in the current study. First, cabin displacement ventilation (CDV) is realized using air distribution bags with an area of 0.88 m^2 mounted below the seats to allow for the injection of air with low momentum (u_{in} < 0.05 m/s), see Fig. 1b). The incoming air generates a ”lake” of fresh air at floor level, from which the air heats up and rises due to buoyancy at the heat sources. At ceiling level, the warm air leaves the cabin through the inversely operated LMCV outlet. Using CDV, very low flow velocities and thus a minimized risk of draft is expected. The second ventilation system is the low momentum ceiling ventilation (LMCV), where a ceiling air outlet (1.16 m^2) allows for both, supply of fresh air at low momentum (u_{in} < 0.04 m/s) and extraction of recirculated air through a trickle ceiling, see Fig. 1c). Finally, a hybrid ventilation (HV) is realized by combining CDV and LMCV, see Fig. 1d). Herewith, 50% of the fresh air is supplied through the CDV inlets and 50% through the LMCV inlets. Again, the extraction is realized using the trickle ceiling.

2.2. Test environment

In order to conduct the required studies, a dedicated full-scale generic car cabin (GCC) was developed and set-up at DLR Göttingen. Its dimensions follow the interior of typical mid-size cars with a surface area of 14.8 m^2 and inner dimensions of 1300 mm (width), 2400 mm (length) and1200 mm (height) (Fig. 2).

The mock-up was built from aluminum profiles and acrylic glass (PMMA, polymethyl methacrylate). To decouple the cabin interior from

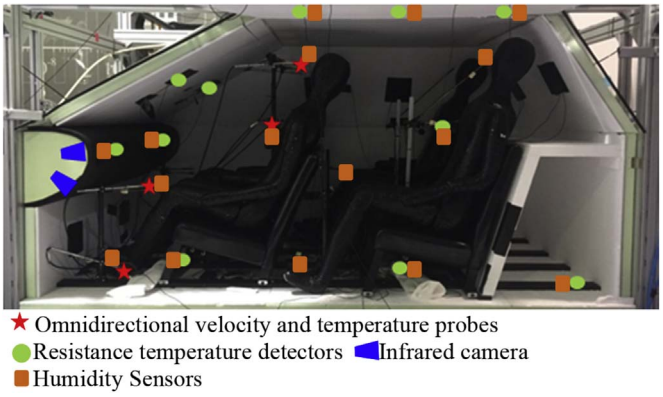

Fig. 2. Side view of the generic car cabin with illustrated sensor positions.

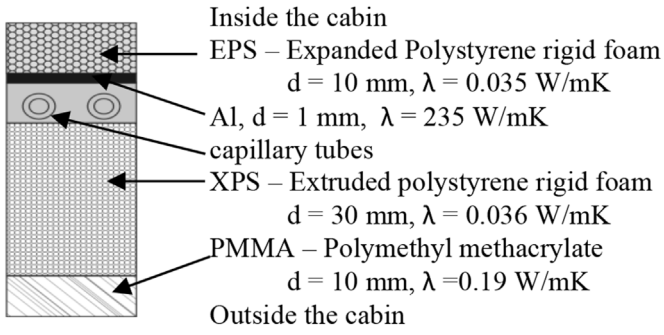

Fig. 3. Cross section of cabin structure with insulation and jacket heating/cooling system. Thickness of each layer and its heat conductivity are given by d and λ, respectively.

the ambient, it was thermally insulated with 50 mm of extruded polystyrene during the measurements of the ventilation efficiency (Section 3.3). A jacket heating/cooling based on capillary tubes connected to an aluminum sheet was implemented in the structure to investigate winter, spring/fall as well as summer conditions, see Fig. 3 (Sections 3.4 and 3.5). For MV, the LMCV outlet was replaced by a jacket heating/cooling at the ceiling. In order to simulate the blockage and the heat release of the passengers, the GCC was equipped with four thermal passenger dummies (TPDs). Each TPD, with a height of 1.73 m and a surface of approx. 1.5 m^2, can be heated by an external power supply. The sensible heat release of each manikin can be varied between 0 and approx. 150 W. It is well known from the literature that the heat release of humans depends on many factors, such as activity, gender, size or ambient temperature For a sitting passenger with normal clothing the values for the latent and sensitive heat release are given e.g. in the standard EN 13129 [24] and confirmed in an experimental analysis within a generic train compartment [25]. However, in the current study, we used a constant value of 75 W for the manikins, well suiting the sensible heat release at a mean cabin temperature of 24.5 °C and previous studies e.g. Refs. [13,19]. For the sake of comparability with the numerical simulations and due to the simultaneous use of the manikins for the acquisition of the equivalent temperature (see Section 2.4), we forgo variations of this value.

Velocities and temperatures in the vicinity of the TPDs were measured using combined omnidirectional velocity and temperature probes (OVTPs). They provide an accuracy of ± 0.02 m/s for the velocity and ± 0.2 °C for the temperature. Further, more than 70 resistance temperature detectors (RTDs) with an accuracy of ± 0.15 K were used to investigate the boundary conditions like air inlet (ϑ_{In}), outlet (ϑ_{Out}) and ambient (ϑ_A) temperatures as well as surface and fluid temperatures at selected positions within the compartment. As Fig. 2 depicts, OVTPs were positioned at four levels in the first row to evaluate temperature stratifications and velocity levels near the TPDs. To observe the boundary conditions of different ventilation systems, temperature probes were also installed in the air inlets and outlets. Surface temperatures were assessed with an infrared (IR) camera, which was installed in the dashboard in the front of the driver TPD. The manikin surface temperatures were used to deduce the local equivalent temperatures in a second step. To investigate the ventilation efficiencies, 20 humidity sensors with an accuracy of ± 1.8% referred to relative humidity were used in air inlets, outlets and in the vicinity of the TPDs. The sensors near the TPDs were installed at ankle, knee, chest and head level, 50 mm away from the surface. The volume flow rate of fresh air was supplied and controlled by a centrifugal fan in combination with a Venturi nozzle. If not indicated otherwise, the volume flow rate amounts to 25 m^3/h/PAX, corresponding to 28 l/s for

four passengers in agreement with [26]. To achieve homogeneous and well-defined air inlet temperatures, we used a fan heater and four computer-controlled Peltier elements. To determine the scaling behavior of the ventilation systems, two higher volume flows (36 l/s, 44 l/s) were considered as well.

Before starting a measurement, the GCC was given at least 120 min of settling time, allowing to reach stable thermal conditions. The results of the temperature and velocity probes were subsequently measured and evaluated over 1200 s at a recording frequency of 1.7 Hz for RTDs and 10 Hz for OVTPs.

2.3. Experimental techniques and methodologies

As a precondition to establish vertical ventilation scenarios, the ventilation performance has to be verified. Hereto, the local mean age of air (LMA, τ_P) as well as the local (LVE, ε_P) and global (η_a) ventilation efficiencies are common figures of merit [27]. The LVE relates the nominal air exchange rate to local mean age of air and characterise the air change effectiveness at a specific location in a compartment. In contrast, the global ventilation efficiency relates the spatially averaged mean age of air in the cabin to the nominal air exchange rate and is thus a measure for the fraction of still waters. For the ease of detection, we used water as tracer gas in a step-down measurement approach [14]. A humidity generator with three ultrasonic nebulizers was used to produce water fog. The tracer gas was introduced and distributed in the GCC until steady local concentrations were observed. After stopping the supply of humidity, its concentration decayed as a result of the air exchange. With the data from the humidity sensors at various positions near the TPD as well as in the air in- and outlets, the LMA and the LVE were calculated following the descriptions of [14]. The global ventilation efficiency was defined according to [12]. During the experimental investigations, utmost care was given to avoid condensation effects within the GCC by choosing the appropriate tracer gas concentrations and temperature levels.

For the evaluation of the thermal passenger comfort, acquisition of single thermal parameters is often insufficient, as it is the interaction of a variety of parameters, such as air temperature, air velocity, surface temperatures and others, which determines the thermal sensation of humans. As an integral quantity, we investigated the equivalent temperature (ϑ_{eq}) to quantify the thermal comfort, see Ref. [13]. Here ϑ_{eq} is defined by the following equation with surface temperature ϑ_s, thermal loss by convection and radiation Q and the combined heat transfer coefficient of radiation and convection h_{cal}.

$$\vartheta_{eq} = \vartheta_s - \frac{Q}{h_{cal}} \tag{1}$$

We enabled measurement of ϑ_{eq} by calibration of a TPD at a heat release rate of 75 W in a thermally isolated, temperature-controlled box following the procedure described in Ref. [20]. However, by enabling temperature control on all walls, we strongly improved the accuracy as compared to the data given in Ref. [20]. The box had dimensions of $1.35 \times 1.35 \times 1.82\ m^3$. We realized different surrounding temperatures by using a jacket temperature control system, which is based on aluminum sheets with attached capillary tubes. 25 RTDs were used to monitor the boundary conditions like fluid and surface temperatures. After a settling time of at least 5 h, the mean surrounding temperature in the isolated box $\langle\vartheta_{Box}\rangle$, which indicates ϑ_{eq}, was calculated. The surface temperatures were determined by high-definition (1280 × 960 px) infrared images, recorded by an infrared camera with a sensitivity of 0.08 K and an accuracy of ± 1.5 K. The accuracy was further improved by offset-calibration of the infrared images using a local RTD on the TPD surface. Calibration curves were generated by measuring the mean surface temperatures of different body parts as a function of the surrounding temperature. The calibration curves reveal linear dependencies of the respective surface temperatures ϑ_S on the mean surrounding temperature $\langle\vartheta_{Box}\rangle$ with slopes very close to unity. Taking into account the limited homogeneity of the temperature in the box and the measurement uncertainties of the surface temperatures, the final accuracy of the equivalent temperatures is estimated to $\Delta\vartheta_{eq} = \pm 0.5$ K.

2.4. Numerical analysis

Besides experimental simulations and measures, numerical simulations were conducted as well. Therefore, a computational fluid dynamics (CFD) model of the GCC was developed including the passenger thermal dummies. The simulations were validated with the experimental data as described in the following, allowing a detailed insight into the three-dimensional flow structures evolving for the different ventilation settings.

To predict the air flow and temperature field in the GCC, the Reynolds-averaged Navier-Stokes (RANS) equations with the Boussinesq approximation were integrated with the "buoyantBoussinesq" solver of OpenFOAM provided by the commercial version of Engys together with the k-Ω/SST turbulence model.

The turbulent equations were solved with second-order linear upwind schemes for turbulence, scalar, vector and radiation fields provided in the source library of Engys edition of OpenFOAM. The equations were discretized and integrated on a hybrid structured/unstructured mesh consisting of a total of approx. 10 million cells which were generated with the mesher of the commercial program StarCCM+. The thermal boundaries were resolved with five wall layers and wall distances in wall units of the grid points next to the walls of $y^+ < 1$ in 92% of the wall cells. The cells have a basic size of 4 mm and a minimal size of 1 mm. These mesh parameters were used together with turbulence models in our former work [28,29]. The presented approach was applied to predict the thermal comfort in aircraft (Do728 and A320) as well as train cabins and was validated by experiments involving test persons. The deviations between experimental and calculated temperatures were found to be in the range of 2–3%.

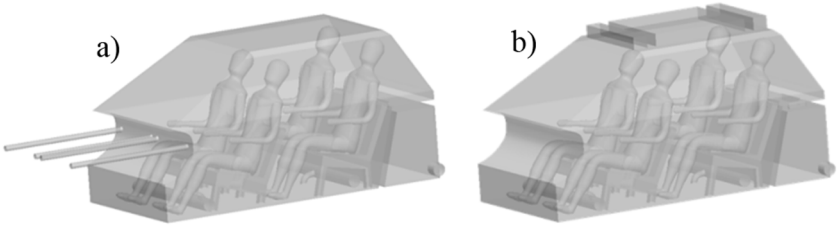

Fig. 4. CFD model of car cabin for a) MV and b) LMCV.

Table 1
Boundary conditions for the different scenarios.

	Winter	Spring/Fall	Summer
$\langle\vartheta_{In}\rangle$ [°C]	25.3	20.4	14.5
$\langle\vartheta_{A}\rangle$ [°C]	7.4	20.4	29.6

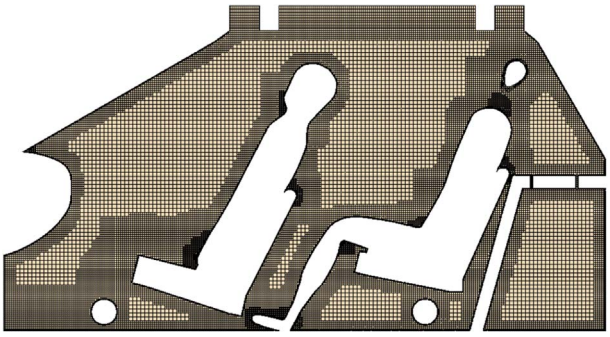

Fig. 5. Cut through unstructured hexahedral mesh for LMCV.

We examined all ventilation variants for winter, spring/fall and summer cases. For this purpose, the inlet air volume rate of 0.028 m^3/s with corresponding initial temperatures (see Table 1) was prescribed and homogeneously distributed over all inlet surfaces. The MV variant has four, CDV two, HV three and LMCV one inlet surfaces (Fig. 1). For a better convergence of the numerical solution, the inlet and outlet surfaces were extruded to the outside for LMCV and HV variants. The resulting CFD models for MV and LMCV variants are presented in Fig. 4. The cross-section of the numerical mesh is shown in Fig. 5.

At the wall, the temperature boundary conditions according to Table 1 were specified. For this purpose the interior wall temperatures measured by experiment, were converted in heat flux densities. These heat flux densities were prescribed at all cabin walls. At the body of manikin, a total heat Q_{total} = 75 W (7.5 W for head and 68.5 W for the rest of the body) was prescribed. The conducted turbulent flow simulations include the computation of heat radiation based on a Discrete Ordinates Model (DOM) with 40 rays. All variants were calculated with the same numeric settings up to 15,000 iterations. By this number of iterations sufficiently converged solutions could be obtained (computed residuals were 5e-4 for velocity and temperature and 2e-6 for pressure).

Before the numerical analysis in the car model, test simulations in the above-mentioned thermal box were performed for three ambient temperatures of 22°, 30° and 35°. This was necessary for the calculation of the heat transfer coefficients h_{cal}. Equation (1) was used in the actual simulations to determine the local equivalent temperatures. The results of the test calculations in the thermal box for temperature were in good agreement with the experiment with an accuracy of 2%.

3. Results

3.1. Thermal boundary conditions of the test cases

Prior to discussion of the actual results, the experimental conditions of the studied test cases will be summarized in this subsection. In order to benchmark the performance of the selected ventilation cases (see Section 2.2), three dedicated thermal scenarios, referred to as “winter”, “spring/fall” and “summer” were considered, see Table 1. They are distinguished by the temperature of the aluminum sheet of the jacket-cooling system, which is considered to represent the outside temperature. In order to adjust the internal cabin temperature to a comfortable level, the inflow temperature was adjusted accordingly.

Due to technical restrictions, however, the actual temperature level deviated from the values given in Table 1. For the winter case, we worked with an air inlet temperature of $\widetilde{\vartheta}_{In}$ = 28 °C and an aluminum sheet temperature of $\widetilde{\vartheta}_{A} = \widetilde{\vartheta}_{Ambient}$ = 10 °C. In contrast, we changed $\widetilde{\vartheta}_{In}$ to 22 °C and $\widetilde{\vartheta}_{A}$ to 37 °C for the summer case. In the spring/fall case, we regulated $\widetilde{\vartheta}_{In} = \widetilde{\vartheta}_{A}$ = 28 °C. However, our TPDs were operated at constant heat flux conditions in contrast to real human subjects. Hence, all temperature differences remained almost unaffected if considered relative to the temperature of the incoming air. For the sake of comparability, we corrected the real boundary conditions with an offset temperature (difference between measured and norm mean equivalent temperature (dashed lines, Fig. 14). Hereto, we considered the mean of the equivalent temperatures of the different ventilation scenarios to determine a common offset temperature for each of the seasonal scenarios. The resulting (corrected) settling temperatures for inlet temperature (ϑ_{In}) and aluminum sheet temperatures (ambient temperature ϑ_{A}) are given in Table 1. As described in Section 2.2, we conducted the studies of the ventilation efficiency without jacket heating/cooling, i.e. at boundary conditions corresponding to the spring/fall case.

3.2. Large scale flow structures and temperature distributions

Before discussing the individual parameters in detail, we would like to give an overview on the large-scale flow structures and temperature distributions resulting from the different ventilation systems and seasonal settings. Hereto, the velocity and temperature color-coded streamlines resulting from the CFD simulations are compiled in Fig. 6.

The velocities and temperatures predicted by CFD are presented exemplarily for the summer case. The colors of the streamlines reflect the velocities a) and the temperature values b). At MV, the flow is dominated by the cooling air jets. Consequently, significantly higher velocities are observed for MV compared to the other ventilation systems. As a result of the high flow velocities, an intense cooling occurs in the torso and arm areas for MV. However, very homogeneous air temperatures are observed. More homogeneous velocity fields are prevailed in LMCV, CDV and HV cases. At pure LMCV, a large-scale circulation develops, delivering the fresh air directly to the passengers in the second row and then to the first row. This issue is resolved at HV, where the fresh air flow is distributed more homogeneously over the inlet surface. In the temperature-coded streamlines, a thermal stratification of increasing strength with rising air fraction through the floor outlets is found. Local reinforcements of the flow velocities, unlikely to stabilize in the real unsteady and highly turbulent cabin flow, unveil the limitations of the steady RANS simulation approach.

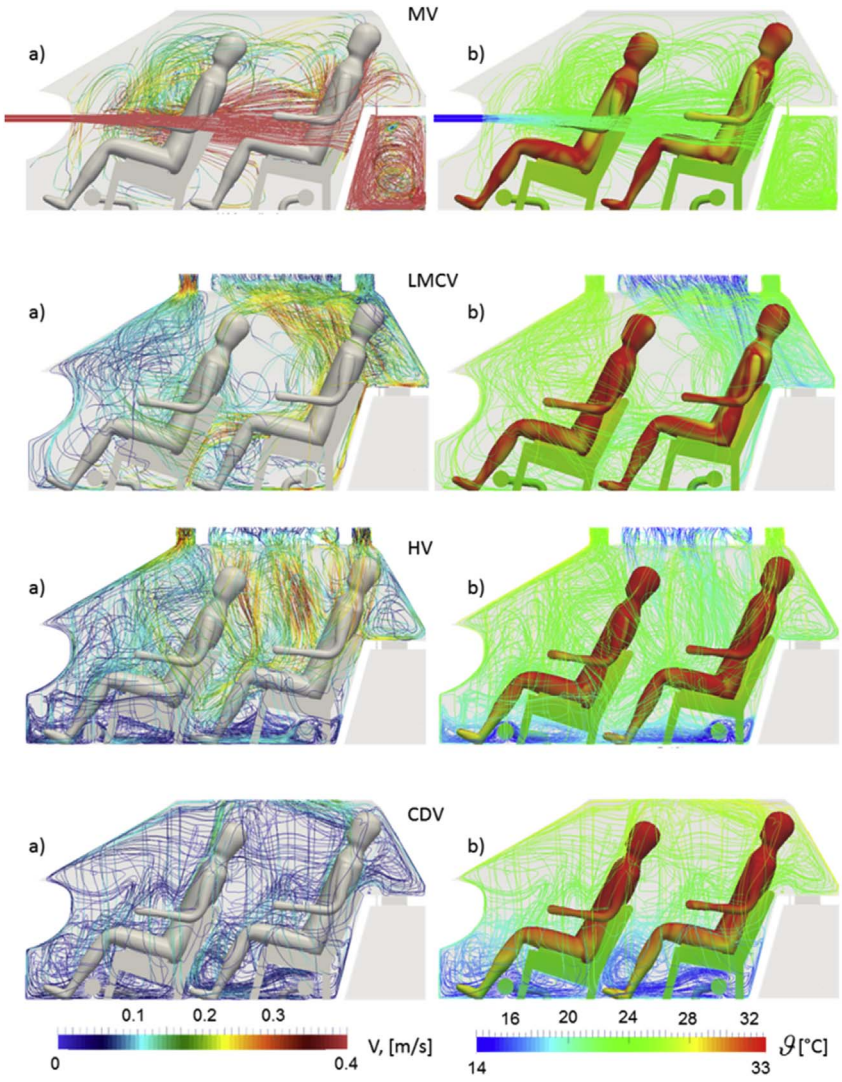

Fig. 6. a) Velocity and b) temperature distributions for all considered variants in summer case.

3.3. Ventilation efficiency

The first parameter to be discussed is the ventilation efficiency, which is a necessary precondition for implementation of vertical ventilation concepts. In the following, we will quantify the ventilation performance by means of the Local Mean Age of air (LMA), the Local Ventilation Efficiency (LVE) and the Global Ventilation Efficiency (η_{Ex}) (see Section 2.3). Before looking at the reduced data, we would like to discuss the LMA as a function of passenger seat and height level exemplarily for HV, see Fig. 7a). Values in the range of 40 s–160 s were found. At head, chest and knee level, the results are similar with respect to the actual seat position. We observe decreasing values from knee to ankle level, where the LMA is 35% lower as compared to the head position. In addition to the LMA, the LVE, relating the nominal time required for a full air exchange to the LMA, is an important measure for the ventilation efficiency.

Fig. 7b) depicts the LVE, again exemplarily for the case of HV, spatially averaged over the four seat positions and height levels for three volume flow rates. The results are very similar for the different volume flow rates, indicating a linear scaling of the LMA with the nominal air exchange time. Only at foot level, a slight increase of the LVE with the volume flow rate is observed.

To benchmark the performance of the different ventilation systems, the spatially averaged LVE in the vicinity of the TPDs is shown for a volume flow rate of 28 l/s in Fig. 8. MV and LMCV reveal a very homogenous LVE of ~1.0. Similar values can be observed for HV at knee, chest and head level. With a rising percentage of air supplied through the displacement ventilation outlets, the LVE increases up to 3.4 at ankle level. For pure CDV, an almost linear dependence from head to ankle with a maximum of 5.6 at the floor level was found. These findings prove, that the convection-driven ventilation scenarios are able to attract the fresh air and concentrate it in the proximity of the passengers, i.e. the boundary layer. Pertaining to all ventilation cases, CDV reveals the best LVE with up to 18% increase in efficiency at breathing level as compared to MV.

As the head level is the most important position regarding air quality, Fig. 9a) compiles the LVE of the different seat positions at head level for a volume flow rate of 28 l/s. MV and HV shine out with very homogeneous results between the different seat positions, while CDV and LMCV provide astonishingly high LVEs in the back seat row.

In addition to the local ventilation measures, the global ventilation efficiency (η_{Ex}) was evaluated to assess the ventilation efficiency in the whole cabin, see Fig. 9b). Values in the range between 50% and 58% can be observed for all ventilation cases and volume flow rates. These values indicate, that none of the ventilation systems tends is likely to generate still waters with locally increased LMA values, i.e. low air quality.

In summary, the vertical ventilation systems provide similar or

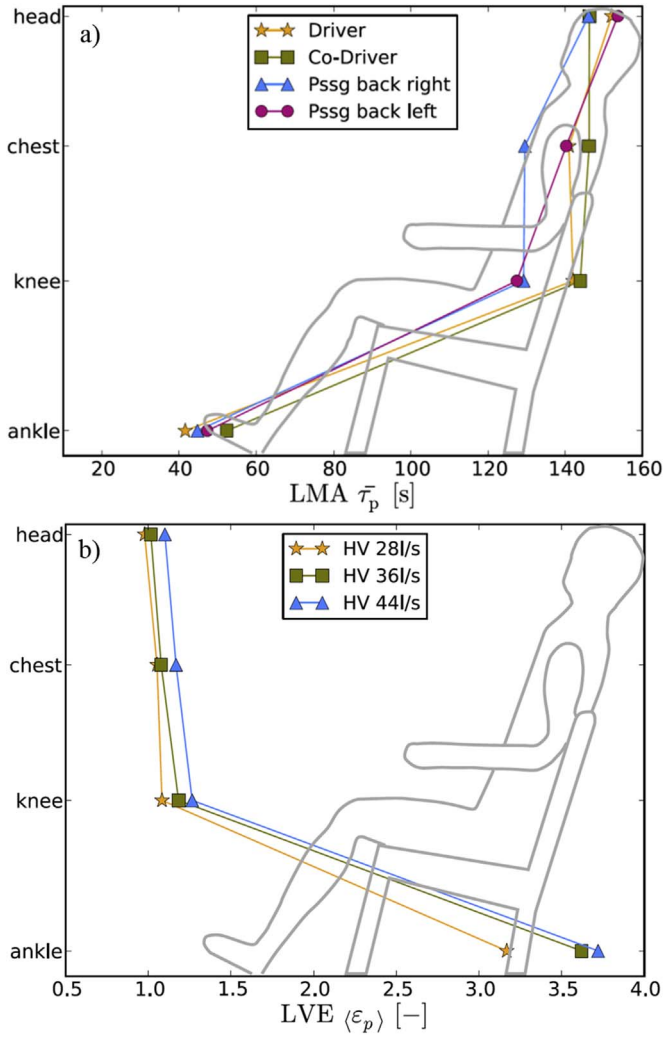

Fig. 7. a) LMA in the proximity of the four TPDs for HV at a volume flow of 28 l/s and b) LVE, averaged over four TPDs for volume flow rates of 28 l/s, 36 l/s and 44 l/s.

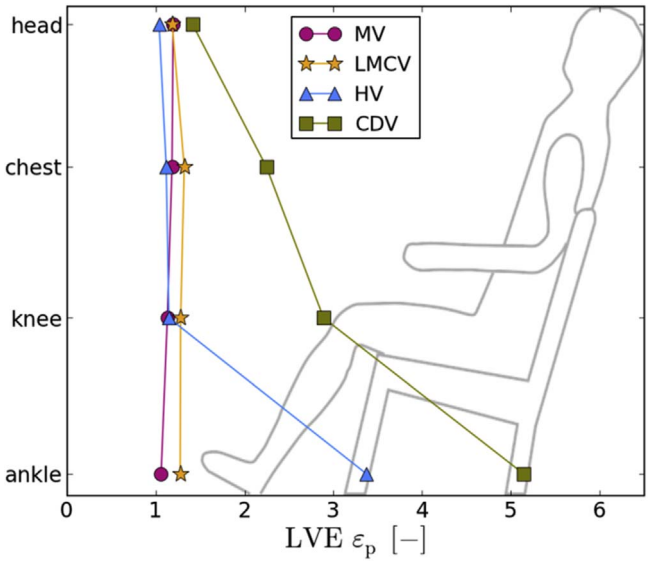

Fig. 8. LVE at different height levels in the vicinity of the TPDs for the investigated ventilation systems at a volume flow rate of 28 l/s averaged over four seat positions.

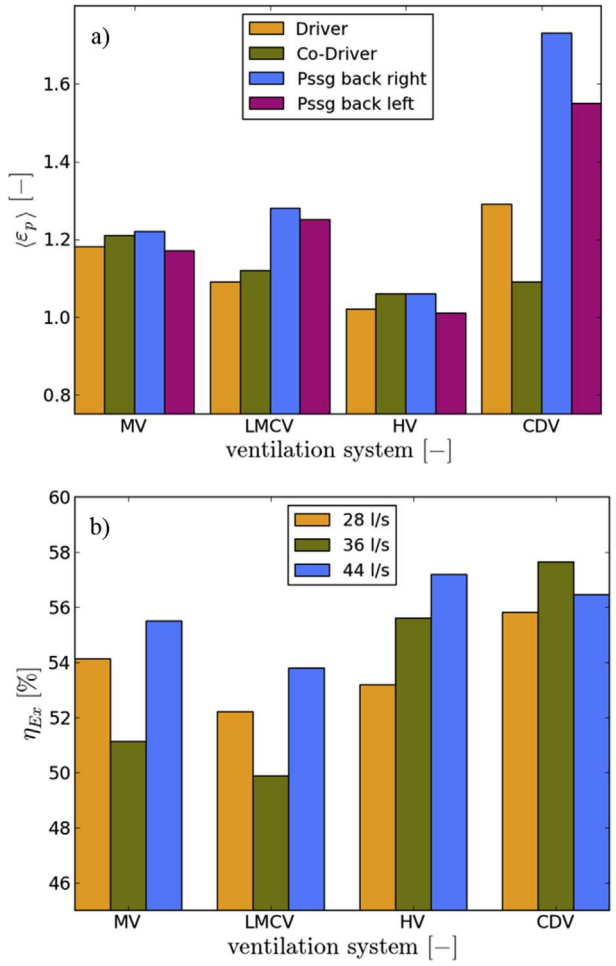

Fig. 9. a) LVE at four head positions for a volume flow of 28 l/s and b) η_{Ex} averaged over four TPDs at three volume flows respectively for different ventilation cases.

better ventilation performance as compared to MV. All systems scale well with the applied volume flow rate. Among the vertical systems, CDV reveals the best results regarding both local and global ventilation efficiency in the generic car cabin.

3.4. Fluid temperatures and velocities

The current section aims at giving an insight into the thermo-fluid dynamical characteristics of the different ventilation concepts at a volume flow rate of 28 l/s. Hereto, temperature and velocity distributions in the GCC are presented. Fig. 10 depicts the mean fluid temperatures, relative to the mean temperature of the incoming air ϑ_{In} in the vicinity of the TPDs for winter and summer conditions. The mean values were determined by temporally averaging over 1200 s at each sensor position and subsequent spatial averaging over the two seat positions in the front row. The results of the CFD simulations are compared representatively to the experimental data.

At winter conditions, stable temperature stratifications can be observed between ankle and chest level. They are smallest for MV and largest for LMCV. Between chest and head level, the temperatures do not change significantly. At summer conditions, MV and LMCV reveal the most homogenous temperature distributions. For CDV, a

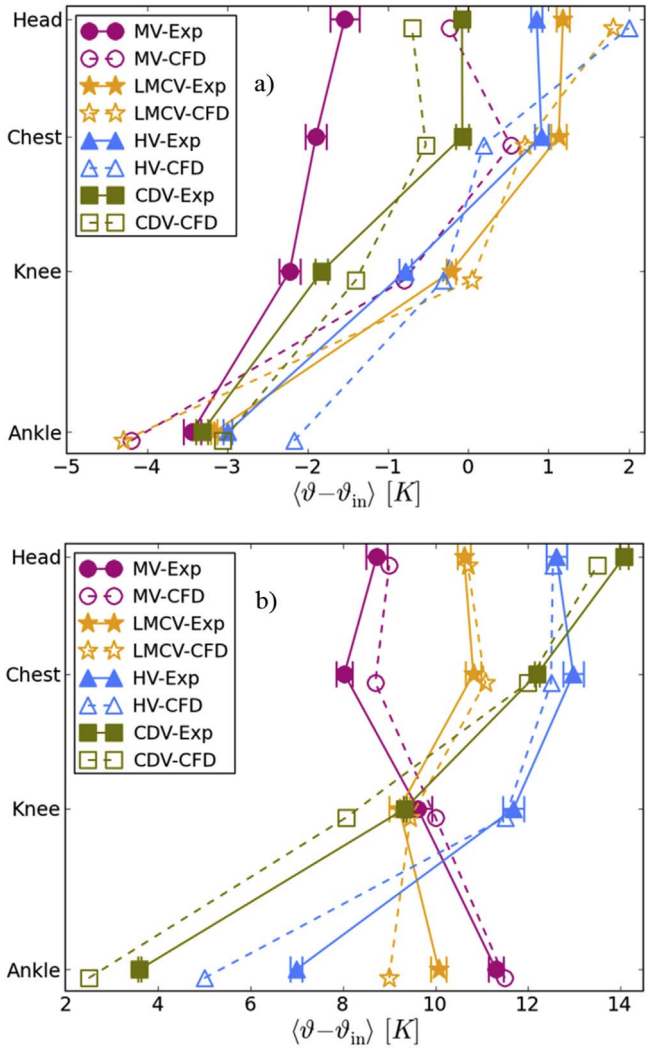

Fig. 10. Mean fluid temperatures at different height levels in the proximity of the TPDs of the front row for a) winter and b) summer conditions. Solid symbols and lines refer to experimental data while open symbols and dashed lines depict results of the CFD simulations.

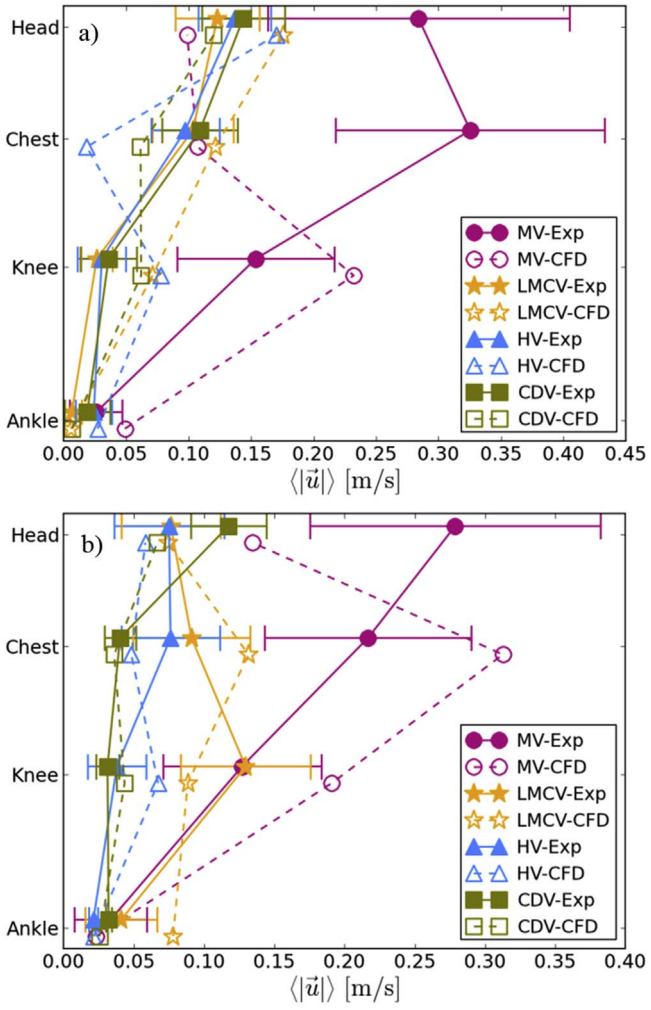

Fig. 11. Mean fluid velocities at different height levels in the proximity of the TPDs of the front row for a) winter and b) summer conditions. Solid symbols and lines refer to experimental data while open symbols and dashed lines depict results of the CFD simulations.

monotonically rising temperature from ankle to head can be detected, which is considerably reduced from 7 K to 5.3 K by the influence of LMCV at HV. The lowest yet unstable temperature stratifications are observed for MV and LMCV. In addition to the average temperatures, their fluctuations, which were not shown for reasons of better recognizability, are important to make a statement on the thermal comfort of the ventilation cases. Here, we observe equal fluctuations for CDV and HV of about 0.1 K, which have predictably a minimal influence on the thermal passenger comfort. The fluctuation rises over 0.17 K for LMCV to a maximum of $\sigma = 0.28$ K for MV. The summer scenarios unveil values of 0.8 K. Similar results are obtained for the other annual scenarios but not shown here for the sake of brevity.

In addition to the local temperatures, the flow velocities in the passenger zone are an important measure to evaluate passenger thermal comfort. Accordingly, Fig. 11 depicts the measured mean fluid velocities for winter (Fig. 11a)) and summer (Fig. 11b)) conditions. Low flow velocities of up to 0.14 m/s in average with standard deviations of up to 0.03 m/s (Table 2) are observed for the vertical ventilation systems. In contrast, MV reveals high mean velocities (0.32 m/s) and velocity standard deviations ($\sigma_{MV} = 0.12$ m/s), outbalancing the

Table 2
Summary of experimental thermo-fluid dynamical flow parameters. Temperature deviations between head and ankle ($\Delta\langle\vartheta_{HA}\rangle$) less than 2.0 K are marked green, $\Delta\langle\vartheta_{HA}\rangle$ deviations larger than 4.0 are marked red [26] and intermediate values in yellow. For the maximal mean velocities ($\langle u\rangle_{max}$), an intermediate section of 0.16 m/s to 0.31 m/s is marked in yellow with lower values highlighted in green and larger velocities in red [26]. Associated fluctuations less than 0.05 m/s are marked green, values between 0.05 and 0.1 yellow and values over 0.1 m/s are marked red.

	Winter				Spring / Fall			
Case	MV	LMCV	HV	CDV	MV	LMCV	HV	CDV
$\Delta\langle\vartheta_{HA}\rangle$ [°C]	2.1	4.4	4.1	3.6	-0.5	1.2	3.5	5.3
$\langle u\rangle_{max}$ [m/s]	0.32	0.12	0.14	0.14	0.27	0.10	0.10	0.15
$\langle\sigma_u\rangle$ [m/s]	0.11	0.03	0.03	0.03	0.10	0.03	0.04	0.03
	Summer							
Case	MV	LMCV	HV	CDV				
$\Delta\langle\vartheta_{HA}\rangle$ [°C]	-2.1	0.4	4.9	10.2				
$\langle u\rangle_{max}$ [m/s]	0.28	0.13	0.08	0.12				
$\langle\sigma_u\rangle$ [m/s]	0.10	0.05	0.04	0.03				

maximum velocity of 0.31 m/s at 26 °C defined as upper threshold in Ref. [26]. All measured values, with exception of the ankle position, are maximal for MV, which indicates the highest kinetic energy of the flow. Comparing experimental and numerical data reveals a heterogeneous picture. While the agreement is quite good for CDV, the results diverge with increasing kinetic energy. Further, the height dependence differs qualitatively. Especially the results for MV indicate deviations in the prediction of the jet propagation. However, on an absolute scale, the RMS deviations of the experimental data are still small amounting to about 0.06 m/s.

To resume the results obtained for the different ventilation scenarios so far, several integral quantities are summarized/given in Table 2. Among them are the maximal mean velocity ($\langle u \rangle_{max}$) and the maximal temperature difference between head and ankle ($\Delta\langle \vartheta_{HA} \rangle$). Conditions with a percentage of dissatisfied of 10% or larger given by Ref. [26] are highlighted in red. These are reached when a vertical temperature difference larger than 4 K or a maximal mean velocity larger than 0.31 m/s occurs. Low vertical temperature differences less than 2 K as well as velocities less than 0.16 m/s are highlighted in green, intermediate values in yellow. A clear dependency of the temperature stratification on the kinetic energy level of the fluid can be detected for all ventilation systems at winter and summer conditions. The maximal vertical temperature difference of 4 K considered a hard limit and was exceeded by LMCV and HV at winter as well as HV and CDV at summer conditions. Obviously, only CDV at winter and LMCV at spring/fall and summer conditions provide satisfying thermal conditions with both, low flow velocities and vertical temperature stratification. However, as the temperature stratification of HV is very close to the limit in both scenarios, further fine tuning of the HV scenario with respect to volume flow rate split and temperature distribution holds provides the perspective of achieving comfortable conditions with this system too.

However, we would like to stress at this point, that this conclusion is drawn on point-wise temperature and velocity measurements only. In the next section, we will address the thermal passenger comfort by incorporating the concept of equivalent temperatures with slightly different findings.

3.5. Equivalent temperatures

While point-wise measurements of flow velocities and temperatures as discussed in the previous section provide a rather indirect means to assess the achievable thermal comfort, evaluation of equivalent temperatures on the TPD surface are considered as an integral method to assess local and global thermal comfort [13]. Hereto, high resolution infrared images of the driver TPD were recorded at stable thermal conditions.

Table 3
Summary of the investigated temperatures by experimental (EXP) and numerical (CFD) study. Temperature deviations of less than 0.5 K are marked green, temperature deviations between 0.5 K and 1 K are marked yellow and deviations of more than 1 K are marked red. For RMS (ϑ_{eq}) between EXP and CFD, values of less than 1.5 K are marked green, between 1.5 K and 2.5 K yellow and higher than 2.5 K are marked red.

	Winter				Spring / Fall			
Case	MV	LMCV	HV	CDV	MV	LMCV	HV	CDV
$\langle\vartheta_{eq}\rangle$EXP [°C]CFD	19.8 21.2	23.2 24.1	22.1 24.2	22.1 23.4	22.2 22.9	25.8 25.7	25.1 24.9	24.1 24.5
RMS (ϑ_{eq}) [K]	2.0	1.3	1.8	1.6	3.4	2.6	1.3	2.0
$\langle\vartheta_{cab}\rangle$EXP [°C] CFD	22.8 23.9	24.8 25.9	24.5 25.8	23.6 24.2	23.9 25.1	25.5 25.6	26.2 24.4	24.6 23.9
	Summer							
Case	MV	LMCV	HV	CDV				
$\langle\vartheta_{eq}\rangle$EXP [°C]CFD	23.2 23.4	25.3 25.1	24.9 24.0	23.6 23.6				
RMS (ϑ_{eq}) [K]	4.3	2.1	1.2	1.3				
$\langle\vartheta_{cab}\rangle$EXP [°C] CFD	24.3 24.9	24.6 24.4	25.4 22.3	24.4 23.2				

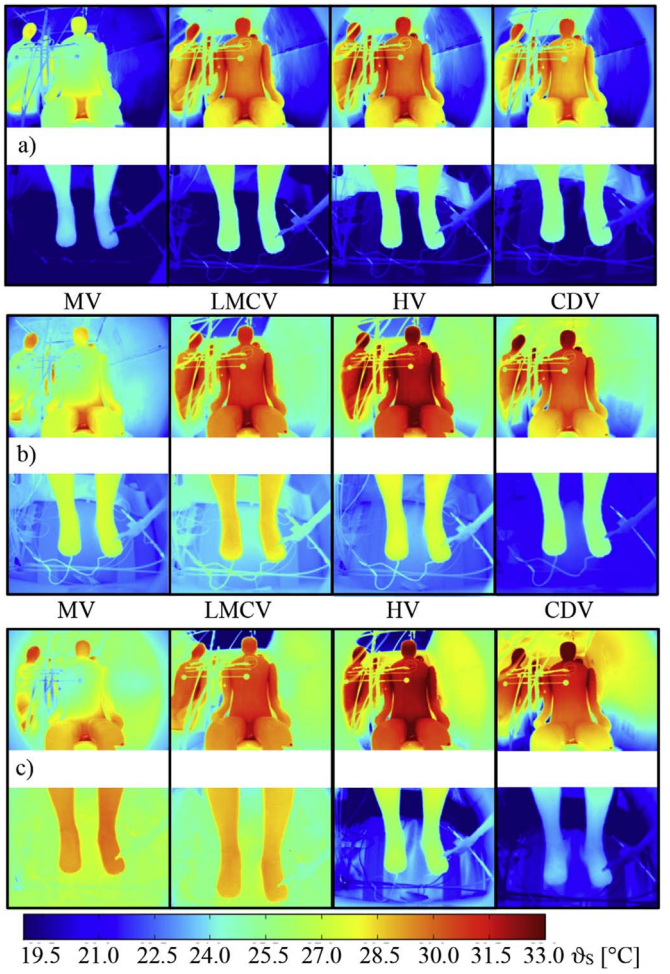

Fig. 12. Infrared views of steady cabin surface temperature distribution, values corrected using the mean norm equivalent temperature for a) winter, b) spring/fall and c) summer condition.

Fig. 12 shows infrared views of the torso region as well as the legs at winter (a)), spring/fall (b)) and summer (c)) conditions. As described at the beginning of Section 3, an offset temperature was subtracted of all pertinent temperatures for the sake of comparability. The corrected values under different environmental conditions as well as a comparison with CFD results are given in Table 3. Here, $\langle\vartheta_{eq}\rangle$ indicates the equivalent temperature and $\langle\vartheta_{cab}\rangle$ the cabin air temperature measured with 8 omnidirectional velocity and temperature probes (see Fig. 2). Comparing the temperatures in the torso region reveals significantly

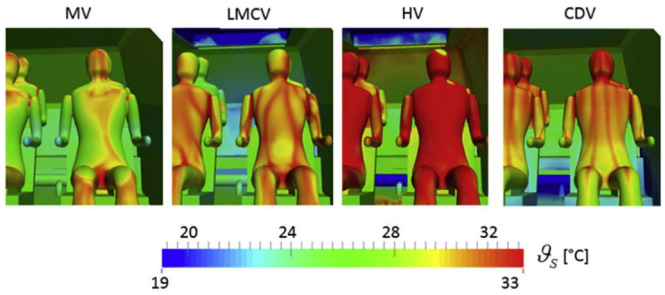

Fig. 13. Distribution of surface temperatures in cabin for summer condition determined numerically.

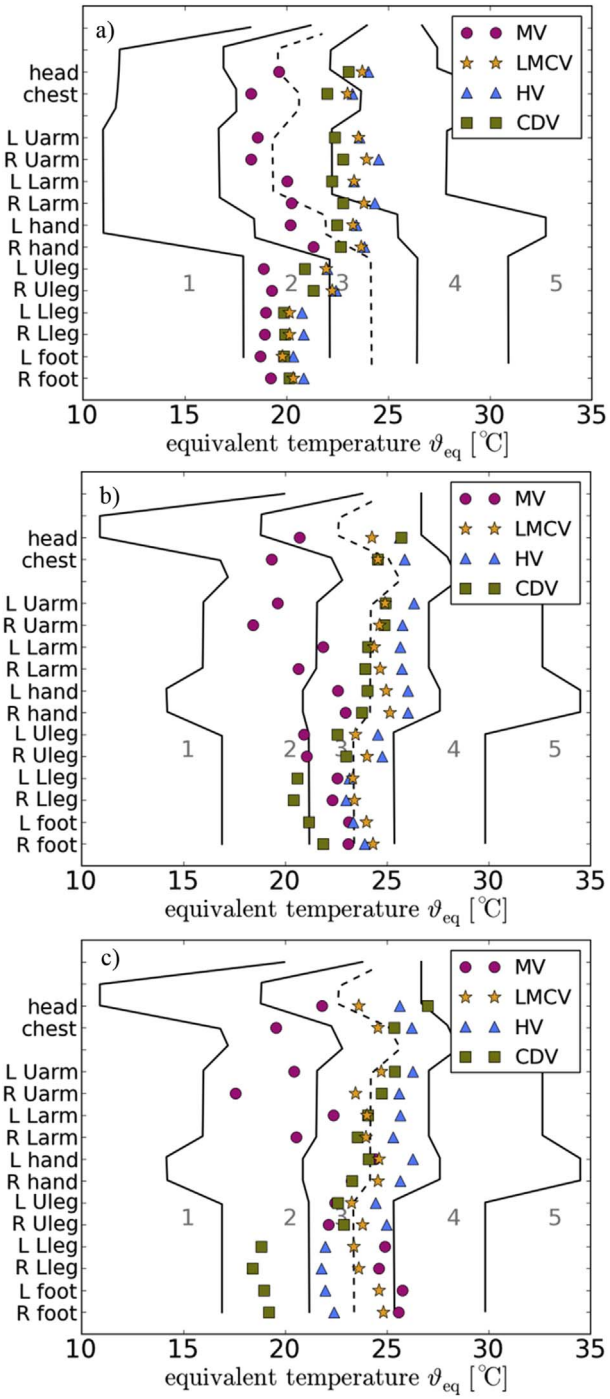

Fig. 14. Experimental results for equivalent temperature of driver-TPD with empiric comfort range for a) winter, b) spring/fall and c) summer condition.

lower dummy temperatures for MV as compared to the vertical ventilation scenarios.

As opposed to real humans, the TPDs are operated under constant heat release conditions. Hence, the reduced surface temperatures at MV in the infrared views as compared to the vertical ventilation systems unveil a higher amount of forced convection at MV. The highest torso temperatures are observed for HV. Characteristic differences between LMCV, HV and CDV can be observed as well: First, lower temperatures atop the head level at LMCV and HV caused by the ceiling air inlet and thus minimal lower head temperatures as compared to CDV. Second, the “lake” of fresh air with lower temperatures in the bottom part is observed for HV and CDV at spring/fall and summer conditions.

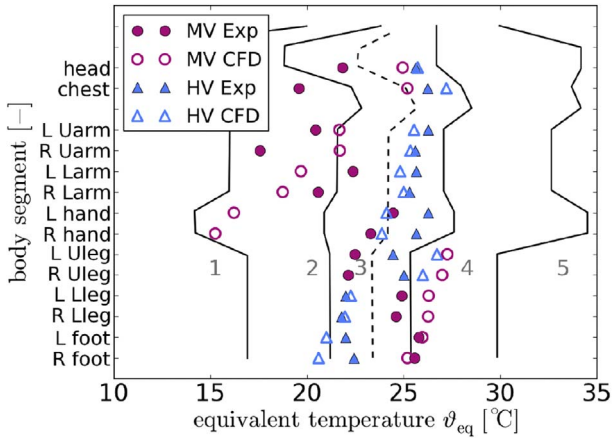

Fig. 15. Experimental and numerical results for equivalent temperatures of the driver TPD with empiric comfort range under summer conditions. Solid symbols and lines refer to experimental data while open symbols and dashed lines in b) depict results of the CFD simulations.

Fig. 13 depicts the cabin surface temperatures for summer condition (CFD). These results reproduce the pictures obtained by experiment quite well (compare with Fig. 12c). From the infrared views, equivalent temperatures were calculated as described in Section 2.3 and equation (1). The results are depicted in Fig. 14 in an empiric comfort range with comfort zones from too cold (1) via neutral (3) to too warm (5) according to [13]. The evaluated body parts are determined by the optically accessible surface areas of the TPD.

Under winter conditions, none of the investigated ventilation systems provides comfortable conditions according to [13], see Fig. 14a). However, benefits of the vertical ventilation systems in terms of heating efficiency, i.e. higher mean equivalent temperatures, can be clearly recognized. Especially HV shines out with the highest mean equivalent temperatures in the winter case. Comfortable conditions in the winter case, however, require higher equivalent temperatures in the lower cabin part. At HV, a correction of low equivalent temperatures in the lower cabin part can be presumably achieved by further fine tuning of air inlet temperatures as well as the split of the volume flow rates between floor and ceiling outlets. We would like to mention, that at MV under winter conditions, normally foot and windscreen nozzles, which we did not implement in the GCC yet, are used for a higher thermal comfort.

Under summer conditions, good thermal passenger comfort is provided by LMCV and HV, see Fig. 14c). Again, further fine tuning of the volume flow rate split or air inlet temperatures at HV will presumably allow for even further improvement of the thermal comfort. MV and CDV on the other hand, shine out with the highest cooling efficiency, which is reflected by the lowest mean equivalent temperatures. Similar results could be observed for the spring/fall case (Fig. 14b) for the upper cabin part. The higher inflow temperature at floor level improves the thermal passenger comfort for CDV and HV at foot and leg position.

Validation of the equivalent temperatures deduced from the CFD simulations with the experimental data reveals a very good agreement for HV under summer conditions, see Fig. 15. The root mean square of the deviations amounts to only 1.2 K. Similar results are obtained for CDV and LMCV, not shown here for the sake of visibility. On the other hand, severe deviations are found for MV, reflecting the differences already observed in the velocity profiles, see Fig. 11. While the mean equivalent temperatures are very similar, the root mean square of the deviations is as large as 4.3 K, indicating deficiencies in the local prediction of equivalent temperatures. For comparison, several integral quantities of experiment and CFD are shown in Table 3, including the RMS values of the deviations between the local equivalent temperatures. The latter unveil, that despite the good agreement between the mean equivalent temperatures, severe differences occur locally, which are reflected in elevated RMS values. The local deviations are especially

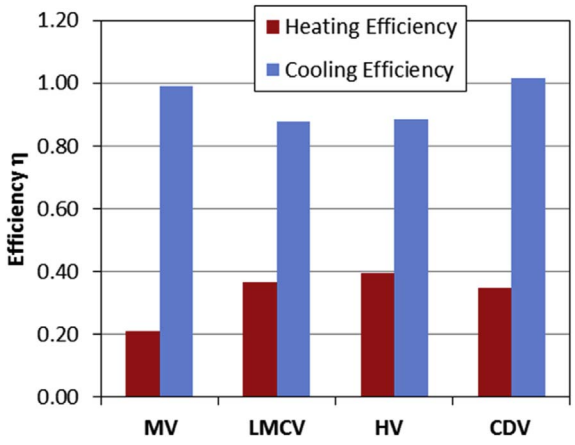

Fig. 16. Heating and cooling efficiency for the winter and summer case, respectively, calculated with (2) using the mean equivalent temperatures from the experimental data.

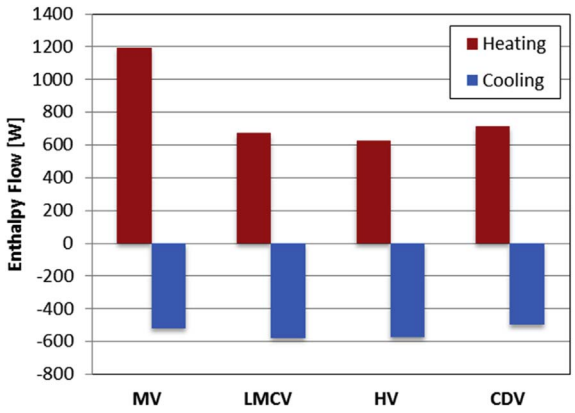

Fig. 17. Enthalpy flows required for heating and cooling during the summer and winter scenarios, referring to an equivalent temperature of 23 °C.

high at MV and LMCV and are considered to be indications of the limitations of the steady simulation approach to representatively predict the paths of the cooling jets as well as the orientation of the large-scale circulations in the cabin.

3.6. Heating and cooling efficiency

As our study aims to improve energetic efficiency, we would like to benchmark the different ventilation cases accordingly in the current section. Hereto we define the *temperature control efficiency* η as the ratio of the air enthalpy flow to the passenger, corrected for its own heating power, and the air enthalpy flow into the cabin:

$$\eta := \frac{\vartheta_{eq} - \vartheta_A - P_H/(q_V \varrho c_p)}{\vartheta_{in} - \vartheta_{amb}} \tag{2}$$

Herewith, P_H, q_v, ρ and c_p denote the total heat load, the volume flow rate as well as the density and specific heat capacity of the air.

The resulting values for η are given in Fig. 16 for the winter and summer case, which is referred to as heating and cooling efficiency in the following. Before we discuss the results, we would like to stress, that η depends on the actual set-point of the system defined by the heat loads, the volume flow rate and, of course, the ambient temperature. In the winter and summer case, the cooling efficiency is significantly higher than the heating efficiency for all ventilation systems, which we ascribe to be an effect of the finite internal thermal insulation of the cabin of about 10 mm polystyrene. Under summer conditions, the TPD surfaces are still warmer than the internal walls, see Fig. 12.

Consequently, cooling of the cabin is supported by heat exchange via radiation between TPDs and walls. The opposite bias occurs under winter conditions: Here, the temperature difference between TPD and cabin surface is even larger, but the resulting heat flux is opposed to the intention to heat the cabin. Looking at the actual values, it turns out, that the vertical ventilation systems show advantages especially under heating conditions, where η is about 90% larger for HV as compared to MV. Under cooling conditions, only CDV is more efficient than MV. Knowing η, we can calculate the actual enthalpy air flow required to heat and cool the cabin by using

$$\dot{H} = (\vartheta_{in} - \vartheta_A)\, q_V \varrho c_p = \frac{(\vartheta_{eq} - \vartheta_A)\, q_V \varrho c_p - P_H}{\eta} + \vartheta_A \tag{3}$$

The resulting enthalpy fluxes to achieve an equivalent temperature of 23 °C are given in Fig. 17. Here, the large differences between heating and cooling scenarios observed in Fig. 16 are put into perspective. The reasons for this are the low values for η in the winter case, which are now compensated by the internal heat loads of the passenger dummies. However, the vertical system HV requires only 52% of the amount of heating power as compared to MV. We ascribe this observation to the fact that MV causes a much higher heat exchange between cabin interior and walls due to forced convection as compared to HV, which is counterproductive in the winter case, and can be circumvented employing optimized, low momentum systems such as HV.

4. Conclusion

Three vertical ventilation concepts for car cabins were investigated experimentally and numerically in comparison to dashboard ventilation (mixing ventilation MV). The vertical concepts comprise a displacement ventilation system (CDV) with air outlets below the seats, low momentum ceiling ventilation system (LMCV) based on a trickle ceiling and hybrid ventilation (HV), a combination of CDV and LMCV. Flow velocities and fluid temperatures in the vicinity of the passenger dummies as well as equivalent temperatures were determined. To experimentally simulate winter, spring/fall and summer conditions, we employed a jacket heating/cooling system. Further, tracer gas measurements were conducted to evaluate the ventilation efficiency.

The performance and comfort relevant parameters evaluated in this paper are rated in Table 4. Concerning the comfort-relevant flow parameters, mixing ventilation shines out with high air velocities and turbulence levels, but homogeneous temperature distributions. The vertical ventilation concepts, on the other hand, allow for comfortable velocity and turbulence levels but tend to develop comfort critical temperature stratifications, except for low momentum ceiling ventilation.

Regarding the equivalent temperatures, none of the ventilation systems was able to provide comfortable conditions according to [13] in the winter scenario. However, the vertical ventilation systems

Table 4
Summary of advantages (+) and disadvantages (−) of different ventilation concepts.[#] Valid for all conditions of the surrounding,* measured for spring/fall conditions only.

	MV	CDV	LMCV	HV
Draft velocity[#]	–	+	+	+
Temperature stratification	o	–	+	–
Summer	o	o	–	–
Winter				
Equivalent temperature	–	o	+	+
Summer	o	o	–	–
Winter				
Local ventilation efficiency*	o	+	o	o
Global ventilation efficiency*	o	+	o	+
Temperature control efficiency	+	+	o	o
Summer	–	+	+	+
Winter				

revealed an improved heating efficiency. To achieve comfortable conditions during the winter time as well, further investigations regarding inlet positions and temperatures are required. In the summer scenario, the highest thermal comfort is provided by LMCV and HV. Especially HV yields further improvement of passenger thermal comfort by adjustments of the volume flow split and outlet temperatures. At MV, reduced equivalent temperatures in the upper cabin part could be observed, which are generated from the high amount of forced convection. Accordingly, MV together with CDV provide the highest cooling efficiency of the passengers under summer conditions, whereas the best thermal comfort is obtained with LMCV and HV.

The vertical ventilation concepts unveil comparable or even better ventilation efficiencies than MV. Especially in the lower cabin part, a better performance of HV and CDV was observed. At head level, CDV shows the best performance with LVEs 50% larger as compared to MV. The global ventilation efficiency ranges between 50 and 60% for all systems and was found to depend on the volume flow rate. HV and CDV reveal the best performance with respect to the global ventilation efficiency.

The results of CFD calculations are partially supported by the experiments. They extend the measurements and allow for a more profound understanding of the nature of the individual variants. However, while the integral quantities, e.g. mean equivalent temperatures, are in quite good agreement with the experimental data, the local deviations of velocities and equivalent temperatures are significant. Hence, on the current basis of numerical simulation, experimental studies have to be considered indispensable. While the aim of the current study was to validate the accuracy level of the present simulation technique, further improvements are envisaged by employing unsteady RANS simulations and temporal averaging. Moreover, a more realistic thermal load was realized in further simulations by the assignment of Thermal Comfort Model [21]. Thus, unsteady simulations with thermal manikins will be considered in future investigations.

Finally, we can summarize, that the vertical ventilation concepts, required e.g. for autonomous driving with rotated front seats, provide many advantages compared to dashboard-based mixing ventilation. Simultaneously, their drawbacks are highlighted, which have to be addressed in upcoming studies. Further, the impact of direct solar radiation has to be addressed in the next step.

An open question is the dynamic performance of vertical ventilation systems such as fast temperature jumps of the incoming air. This topic and a more detailed characterization and quantification of the vertical ventilation systems will be addressed in future studies. Furthermore, variations of the volume flow distributions and air inlet temperatures at HV, promising an increased thermal comfort, will be analyzed.

References

[1] C.C. Chan, Y.S. Wong, Electric vehicles charge forward, IEEE power & energy Mag. 2 (2004) 24–33.

[2] O. Egbue, S. Long, Barriers to widespread adoption of electric vehicles: an analysis of consumer attitudes and perceptions, Energy policy 48 (2012) 717–729.

[3] J.T. Lee, S. Kwon, Y. Lim, M.S. Chon, D. Kim, Effect of Air-conditioning on Driving Range of Electric Vehicles for Various Driving Modes, SAE Technical Paper (2013).

[4] A. Haakana, J. Laurikko, R. Granström, R. Hagman, Assessing Range and Performance of Electric Vehicles in Nordic Driving Conditions, End of Project Report; RekkEVidde project Norden Energy & Transport, 2013.

[5] A. Frohmer, D. Dvorak, T. Bäuml, D. Simic, Novel heating concept for full electric vehicles, Elektrotechnik Inf. 132/3 (2015) 168–171.

[6] S. Krome, W. Goddard, S. Greuter, S.P. Walz, A. Gerlicher, A context-based design process for future use cases of autonomous driving: prototyping AutoGym, Proceedings of the 7th International Conference on Automotive User Interfaces and Interactive Vehicular Applications, 265–272, 2015.

[7] C. Diels, J.E. Bos, Self-driving carsickness, Appl. Ergon. 53 (2016) 374–382.

[8] M.C. Da Silva, Measurement of comfort in vehicles, J. Meas. Sci. Technol. 13 (2002) R41.

[9] J.P. Lee, H.L. Kim, S.J. Lee, Large-scale PIV measurements of ventilation flow inside the passenger compartment of a real car, J. Vis. 14 (4) (2011) 321–329.

[10] J. Rosendahl, B.W. Olesen, Comparison of temperature measurement methods for evaluation of the thermal environment in vehicles, Int. J. Veh. Des. 42 (1–2) (2006).

[11] T. Madsen, B. Olesen, K. Reid, New Method for Evaluation of the Thermal Environment in Automotive Vehicles, Danmarks tekniske hojskole, laboratoriet for varmeisolering, 1986.

[12] A. Wesseling, J. Niebel, K. Rewitz, B. Flieger, M. Schmid, D. Müller, Measurement System for Air Change Effectiveness in Car Cabins, FISITA2014 World Automotive Congress, Maastricht, the Netherlands (June 2-6 2014).

[13] ISO 14505-2, International Standardization Organization 14505-2, (2006).

[14] H. Han, Ventilation effectiveness measurements using tracer gas techniques, InTech 3 (2012) 41–66.

[15] J. Bosbach, S. Lange, T. Dehne, G. Lauenroth, F. Hesselbach, M. Allzeit, Alternative ventilation concepts for aircraft cabins, CEAS Aeronautical J. 4 (2013) 301–313.

[16] A. Wang, Y. Zhang, Y. Sun, X. Wang, Experimental study of ventilation effectiveness and air velocity distribution in an aircraft cabin mockup, Build. Environ. 43 (2008) 337–343.

[17] T. Zhang, Q. Chen, Novel air distribution systems for commercial aircraft cabins, Build. Environ. 42 (2007) 1675–1684.

[18] S. Yin, T. Zhang, A New under- Aisle Displacement Air Distribution System for Wide- Body Aircraft Cabins, Eleventh International IBPSA Conference, Glasgow, Scotland (July 27-30, 2009).

[19] T. Dehne, A. Volkmann, D. Schmeling, J. Bosbach, Experimental analysis of different ventilation concepts for the passenger compartment of a generic car, Proceedings of the 14th Indoor Air Conference, Ghent, Belgium, July 3-8, 2016.

[20] T. Dehne, P. Lange, A. Volkmann, D. Schmeling, J. Bosbach, Ventilation efficiency and thermal passenger comfort of novel car ventilation concepts, Proceedings of ASHRAE Conference, Los Angeles, United States, June 24-28, 2017.

[21] M. Konstantinov, C. Wagner, Numerical simulation of the thermal comfort in a model of a passenger car cabin; new results in numerical and experimental fluid mechanics X, Notes Numer. Fluid Mech. Multidiscip. Des. 132 (2016) 383–393.

[22] N. Boughanmi, L. Enke, J. Frisch, C. van Treeck, Numerical evaluation of vertical air ventilation systems for future car cabins, Proceedings of the 14th Indoor Air Conference, Ghent, Belgium, July 3-8, 2016.

[23] T. Zhang, L. Tian, C.-H. Lin, S. Wang, Insulation of commercial aircraft with an air stream barrier along fuselage, Build. Environ. 57 (2012) 97–109.

[24] EN 13129, Railway Applications; Air Conditioning for Main Line Rolling Stock, Comfort Parameters and Type Tests, 2016. German Version EN 13129:2016.

[25] D. Schmeling, J. Bosbach, On the influence of sensible heat release on displacement ventilation in a train compartment, Build. Environ. 125 (2017) 248–260.

[26] ASHRAE, 2001 ASHRAE Handbook of Fundamentals, American Society of Heating, Refrigerating and Air Conditioning Engineers, Inc, Atlanta, GA, 2001.

[27] Y. Zhang, Indoor Air Quality Engineering, ISBN 1-56670-674-2 CRC Press LLC, Washington, 2005.

[28] M. Konstantinov, W. Lautenschlager, A. Shishkin, C. Wagner, Numerical simulation of the air flow and thermal comfort in aircraft cabins; new results in numerical and experimental mechanics IX, Notes Numer. Fluid Mech. Multidiscip. Des. 124 (2014) 293–302.

[29] M. Konstantinov, C. Wagner, Numerical simulation of the thermal comfort in a train cabin, Int. J. Railw. Technol. 4 (2015) 3.